Progress In Electromagnetics Research, Vol. 139, 193–209, 2013

MODELING AND ANALYSIS OF CONDUCTED ELECTROMAGNETIC INTERFERENCE IN ELECTRIC VEHICLE POWER SUPPLY SYSTEM

Yan Jie Guo, Li Fang Wang*, and Cheng Lin Liao

Key Laboratory of Power Electronics and Electric Drive, Institute of Electrical Engineering, Chinese Academy of Sciences, No. 6 Beiertiao, Zhongguancun, Beijing, China

Abstract—Electromagnetic interference (EMI) of the power supply system in electric vehicles will seriously affect the safety of the vehicle and passengers' health. So a model of power supply system is presented to analyze its conducted EMI in the paper. This model shows the effects of paralleled interleaving DC/DC converter, which contains the new circular current EMI characteristics. Also, a novel power battery model is established considering both the energy dynamic processes and the high frequency features. Firstly, the power electronics devices are studied as the most important part of the DC/DC converter. Then, the equivalent model of the paralleled interleaving DC/DC converter is set up to express the interference source features. Also, the power battery, which is the main energy storage equipment in electric vehicles, is modeled as EMI propagation paths. Furthermore, loads of the power supply system, such as lead acid battery and low voltage devices, are investigated to evaluate their immunity. Finally, the system model is established. The system EMI is analyzed to get their generating causes, time domain and frequency domain characteristics based on both simulations and experiments.

1. INTRODUCTION

There are severe electromagnetic compatibility (EMC) problems in electric vehicles because of high voltage equipment, such as power electronics converters, electric motor and so on. Also, electromagnetic pulses will appear when the vehicle starts or changes working conditions. They will bring electromagnetic interference (EMI) to low

Received 11 March 2013, Accepted 15 April 2013, Scheduled 24 April 2013
* Corresponding author: Li Fang Wang (wlf@mail.iee.ac.cn).

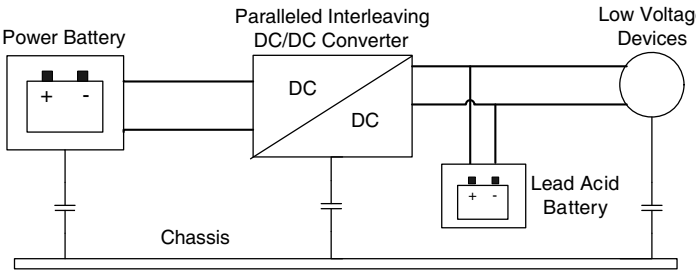

Figure 1. Power supply system in one kind of electric vehicle.

voltage devices. Since many low voltage devices are important control or implementation units, once disturbed, the stability of the vehicle and the safety of passengers will be affected. So these problems are related to the efficiency and reliability of electric vehicle power systems, which are focused on by researchers in recent years [1].

In order to investigate EMC problems in power supply system, its composition should be made clear. The power supply system used in one kind of electric vehicle is shown in Fig. 1. The paralleled interleaving DC/DC converter is the interference source in this system. The power battery is the main energy storage equipment and also the EMI propagation path. The loads contain the lead acid battery and low voltage devices. The former is the auxiliary energy storage equipment; the latter include many electric control units (ECUs) in electric vehicles, such as battery management system (BMS), vehicle controller, etc.

EMI in electric vehicles can be studied through numerical algorithms of electromagnetic fields, such as finite difference time domain (FDTD) method [2, 3], finite element method (FEM) [4, 5], etc. Also, there are some literature investigated on conducted EMI in other power systems [6]. The power converter model and common mode (CM) current analysis [7] in the literature can be extended to the EMI research on the power supply system in electric vehicles.

There are some papers focusing on conducted EMI in electric vehicles [8, 9]. Some study the interference characteristics by using the EMC model of the power converter and the motor [10, 11]. But they ignore stray parameters of power converters. This will lead to inaccurate results, especially in the high frequency range where couplings and resonances caused by stray parameters are dominant. Another research gives the high frequency model of equipments in electric vehicles considering the stray parameters [12]. Nevertheless, it does not express the effects of the battery. Some models of the power battery are established based on the electrochemical

features [13, 14]. However, these models cannot express the high frequency characteristics, which are very important for interference analysis. For some high frequency models [15], they do not consider the energy storage state, which will affect the parameters of the power battery.

Based on the research above, the power supply system of electric vehicles is modeled, and its EMI characteristics are shown in this paper. This model considers the effects of circular current EMI in paralleled interleaving DC/DC converter which has been neglected by the previous research. Also, a novel power battery model is included, which express the electrochemical and high frequency features of the power battery more accurately. Furthermore, the high frequency models of lead acid battery and BMS are studied as the EMI propagation paths. Their impedances are expressed to evaluate their immunity. These analyses provide a way to present EMC characteristics of high voltage and low voltage equipments in one system. Also, they make the EMI sources, propagation paths and sensitive devices clear, and make it easy to develop the suppression programs. So in this paper, the paralleled interleaving DC/DC converter is analyzed as the EMI source firstly. Then, the power battery is modeled and the parameters are identified. Also, the lead acid battery and BMS are considered as the loads. Finally, the system model is established and the differential mode (DM) and CM EMI characteristics are obtained from the simulations and experiments.

2. PARALLELED INTERLEAVING DC/DC CONVERTER

2.1. Power Electronics Devices

Essentially, the EMI in DC/DC converter is caused by switching processes of power electronics devices. The turn-on and turn-off behaviors of power electronics devices can be obtained from experiments [16] and approximately divided into different stages [17]. Also, inductances of the connected wires [9], coupling capacitances and other stray parameters are considered to get the equivalent models [12]. However, this kind of complex model will bring a large number of calculations and the details of switching processes may not affect much from the system point of view. So they are ignored and only the simple switching processes are described in this paper.

There are two kinds of power electronics devices in DC/DC converter: one is metal oxide semiconductor field effect transistor (MOSFET); the other is power diode. Firstly, the interference source feature of MOSFET is discussed. The time domain on-off processes of

MOSFET can be described as trapezoidal pulses [18]. Assuming the turn-on time is the same with the turn-off time, the trapezoidal pulses will have the same rising and dropping edges. The frequency domain expression of this kind of trapezoidal pulses is given by Eq. (1). Where, $A_{\max}$ is the amplitude of the trapezoidal pulses; T is the switching period of the MOSFET; d is the turn-on and turn-off time; k is the order of the harmonics based on the switching frequency.

$$F(k) = \frac{4A_{\max}}{\pi}\frac{T}{2\pi d}\frac{1}{k^2}\left|\sin\left(k\frac{2\pi d}{T}\right)\right| \tag{1}$$

Then, the interference characteristic of power diode is shown. Unlike MOSFET, most interference of power diode is caused by its reverse recovering current. The reverse recovering current contains the following important parameters: amplitude I_{tt}, reverse recovering time t_{rr}, rising time t_r and dropping time t_d. Their relationships and values will be totally or partly given in the product data sheet. In the time domain, the reverse recovering current can be approximately equivalent to a triangle wave, with the bottom t_{rr} and the high I_{tt}. Assuming $t_r = t_d$, the frequency domain expression of the reverse recovering current is given by Eq. (2). Where, f_s is the switching frequency of the MOSFET; k is the order of the harmonics based on the switching frequency.

$$F(k) = I_{rr}f_s t_{rr}\left(\sin\left(\frac{\pi k f_s t_{rr}}{2}\right)\Big/\frac{\pi k f_s t_{rr}}{2}\right)^2 \tag{2}$$

Finally, the interference of MOSFET can be equivalent to an interference voltage source, and the interference caused by reverse recovering current of the power diode can be equivalent to an interference current source. They can be represented by Eqs. (1) and (2) in the frequency domain.

2.2. Converter Model

A conducted interference model of the basic topology of DC/DC converter used in electric vehicles is shown in [12], and the on-board charger is discussed in [19]. However, there are circular currents flowing through the two paralleled parts of the paralleled interleaving DC/DC converter. This is because the on-off waveforms of the two power electronics devices have a phase difference of $\pi/2$. Also, the system interferences will be different on the effects of the interleaving control method. So in order to analyze the new EMI characteristics, the topology and stray parameters of the paralleled interleaving DC/DC converter should be considered to build a new converter model.

The equivalent model of the paralleled interleaving flyback DC/DC converter used in electric vehicles is shown in Fig. 2, where U_{g1} and U_{g2} are equivalent voltage sources of MOSFETs; I_{d1} and I_{d2} are equivalent current sources of power diodes; T_1 and T_2 are ideal transforms with turns radio n; L_1 and L_2 are equivalent inductances of the transforms; R_{11} and R_{21} are equivalent resistances in transform primary sides; R_{12} and R_{22} are equivalent resistances in transform secondary sides; C_L is the output capacitance; Z_{bat} is the equivalent impedance of the power battery; Z_{load} is the equivalent impedance of the loads; C_1-C_4 are the coupling capacitances between the primary sides and secondary sides of the transformers; C_g is the coupling capacitance between the converter and the ground; L_{cable} is the equivalent inductance of connecting cables; R_{com} and L_{com} are the equivalent impedances of CM interference propagation paths.

The values of the parameters in Fig. 2 can be obtained from measurements and equivalent calculations. Their values are given in Table 1.

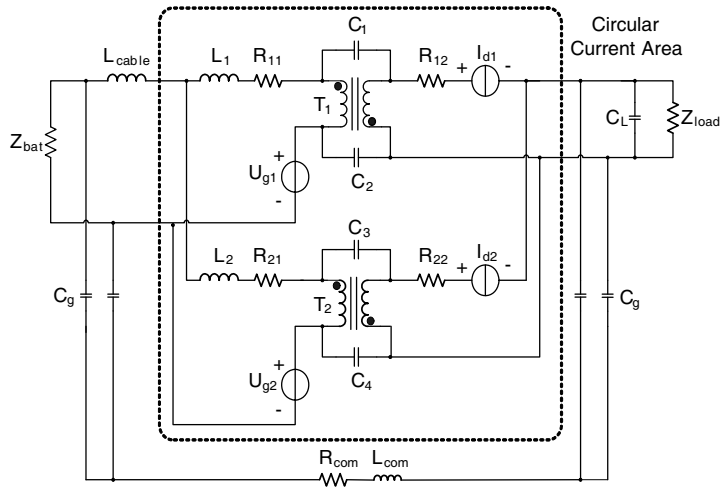

Figure 2. Equivalent model of the paralleled interleaving DC/DC converter.

Table 1. Values of the parameters in the model in Fig. 2.

L_1, L_2	R_{11}, R_{12}	R_{21}, R_{22}	C_L
1.1 mH	0.276 Ω	0.017 Ω	2200 μF
C_1-C_4	C_g	L_{cable}	R_{com}, L_{com}
1 nF–10 nF	10 nF–100 nF	120 nH	≈ 0.01 Ω, ≈ 10 nH

Figure 2 infers that there are two kinds of EMI in the paralleled interleaving DC/DC converter. One is the system input and output EMI, which influences the equipments which are connected with the DC/DC converter. It is related to the superposition of the two paralleled parts' interference sources as shown in Fig. 2. Because the interleaving control, the interference source waveforms of the two paralleled parts have a phase difference of $\pi/2$. So the odd-numbered harmonics of the MOSFET switching frequency are cancelled. Hence, the interleaving control can reduce the output ripples [20]. The other kind of EMI is circular current interference which will be discussed as follows.

2.3. Circular Current EMI Analysis

The circular current EMI only flows through the two paralleled parts and does not conduct out of the DC/DC converter. But these circular currents will increase the power losses and cause radiation emissions to affect low voltage equipments in electric vehicles. The circular current EMI can be divided into DM part and CM part. Firstly, the DM part is analyzed. Because the coupling capacitances are very small, they can be neglected in the DM part analysis. So based on the circular current area shown in Fig. 2, the equivalent circuit of DM circular current can be given in Fig. 3.

As shown in Fig. 3, i_{cir} is the DM circular current in the primary side of the transform and its expression can be given by Eq. (3).

$$I_{cir}(j\omega)=\frac{U_{g2}(j\omega)-U_{g1}(j\omega)}{R_{11}+R_{21}+j\omega(L_1+L_2)+\frac{R_{12}}{n^2}+\frac{R_{22}}{n^2}}+n(I_{d2}(j\omega)-I_{d1}(j\omega)) \quad (3)$$

Equation (3) suggests that the superposition of two paralleled parts' interference sources causes the DM atcircular current. Because the inductances of the transforms are usually large and increase with frequency, the EMI of MOSFETs will be weakened in the DM circular currents, while the EMI of power diodes is amplified n times on the effect of the transformers.

Then, the CM part is investigated. It mainly propagates through the coupling capacitances between the primary sides and secondary sides of the transformers. So based on the circular current area shown in Fig. 2, the equivalent circuit of CM circular current can be given in Fig. 4.

As shown in Fig. 4, i_z is the CM circular current, and its expression can be given by Eq. (4), where "//" means that the two impedance variables are parallel.

Equation (4) suggests that the CM circular current is also caused by the superposition of two paralleled parts' interference sources.

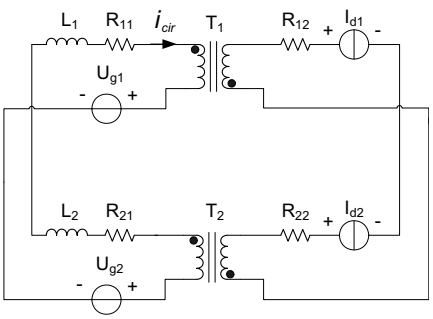

Figure 3. Equivalent circuit of DM circular current EMI.

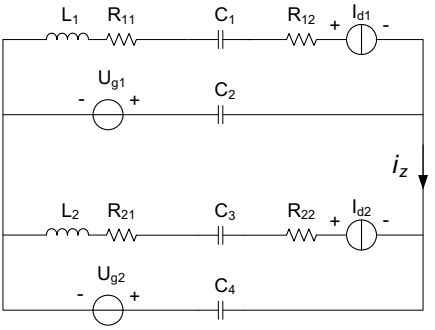

Figure 4. Equivalent circuit of CM circular current EMI.

However, it depends more on the coupling capacitances C_1-C_4. Because the coupling capacitances are very small, there will be only a few CM circular current EMI. Also, the resonances of C_1-C_4, stray inductances, and resistances will affect the high frequency features of the CM circular current EMI.

$$\begin{aligned} i_z(j\omega) = & \frac{\frac{1}{j\omega C_4}}{Z_{p2} // \frac{1}{j\omega C_2} + \frac{1}{j\omega C_4}} * I_{d2}(j\omega) - \frac{\frac{1}{j\omega C_2}}{Z_{p1} // \frac{1}{j\omega C_4} + \frac{1}{j\omega C_2}} I_{d1}(j\omega) \\ & + j\omega(C_2 + C_4)(U_{g1}(j\omega) - U_{g2}(j\omega)) \end{aligned} \tag{4}$$

$$Z_{p1} = R_{21} + R_{22} + j\omega L_2 + \frac{1}{j\omega C_3}, \quad Z_{p2} = R_{11} + R_{12} + j\omega L_1 + \frac{1}{j\omega C_1}$$

3. POWER BATTERY

3.1. Equivalent Model

Power battery is one of the principal propagation paths for conducted EMI. Also, as the main energy storage equipment in electric vehicles, its parameters change with the energy storage state, which can be expressed by state of charge (SOC) of the power battery. Based on the estimation of SOC, the equivalent model of the power battery can be established [13]. In this model, internal resistance and self-discharge effects are considered [14]. Also, inertia resistance and capacitance (RC) sections are used to simulate polarization effects [21]. But this model does not contain the high frequency features of the power battery. The frequency-depended impedances and stray parameters are included in the high frequency model [15, 18]. The parameters of the power battery should be functions of both SOC and frequency. Based on these researches, a more accurate power battery model is

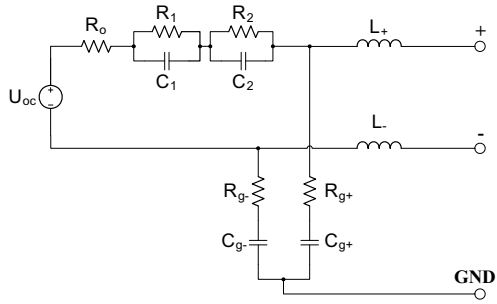

Figure 5. Equivalent circuit model of the power battery.

put forward in this paper.

The power battery model is shown in Fig. 5, where U_{oc} is the open circuit voltage; R_0 is internal resistance; the two RC sections are used to express polarization effects; L_+ and L_- are inductances of connecting cables; C_{g+}, R_{g+}, C_{g-}, R_{g-} are CM coupling parameters between power battery and the ground. Besides, the parameters of the power battery itself are the functions of SOC. Also, the inductances and capacitances change with frequency.

3.2. Model Parameter Identifications

The parameters of the power battery itself (U_{oc}, R_0, R_1, C_1, R_2, and C_2) can be identified based on the hybrid pulse power characterization (HPPC) test [22]. The test object is a kind of 66 Ah $LiFePO_4$ power battery used in electric vehicles. It has six single batteries in parallel in each battery module and has 600 single batteries in total. The test equipment is one kind of battery charging and discharging equipment manufactured by Arbin Company. The test temperature is 25°C. The test data and corresponding fitting curves are shown in Fig. 6. The fittings are achieved by three order polynomials. These figures suggest that the impedances are functions of the power battery SOC.

Considering the skin effect of the power battery, the internal resistance will change with frequency [8]. Its expression is given by Eq. (5), where σ_{skin} is the skin effect coefficient related to the power battery length, cross-sectional area and material features.

$$\begin{aligned} & R_0(f, SOC) \\ &= \sigma_{skin} f * \left(-0.06 * SOC^3 + 0.19 * SOC^2 - 0.20 * SOC + 0.27\right) \end{aligned} \quad (5)$$

Furthermore, the capacitance parameters vary from frequency, and they are functions of both SOC and frequency. According to the fitting results, the expressions of polarization capacitances C_1 and C_2

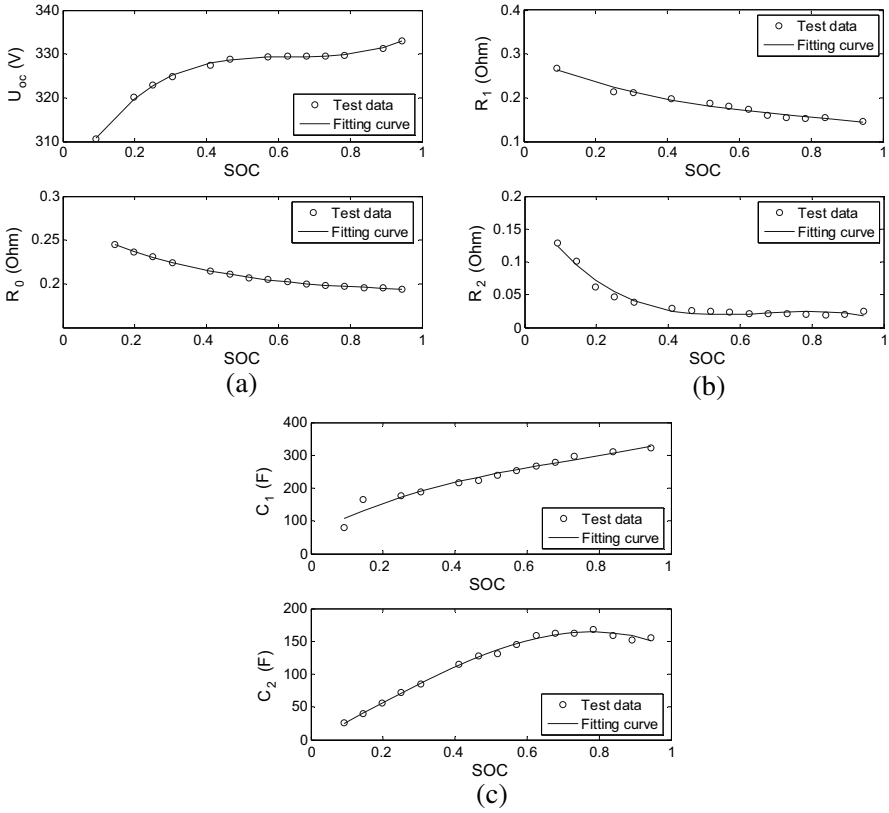

Figure 6. Parameter test and fitting results of the power battery model, (a) U_{oc} and R_0, (b) R_1 and R_2, (c) C_1 and C_2.

are given by Eq. (6).

$$\begin{aligned} &C_1(f, SOC) \\ &= \frac{1}{j2\pi f * (255.28 * SOC^3 - 549.29 * SOC^2 + 576.47 * SOC + 58.54)} \\ &C_2(f, SOC) \\ &= \frac{1}{j2\pi f * (-239.91 * SOC^3 + 103.99 * SOC^2 + 276.29 * SOC - 0.42)} \end{aligned} \tag{6}$$

The parameters of connecting cables (L_+, L_-) and CM coupling capacitances, resistances (C_{g+}, R_{g+}, C_{g-}, R_{g-}) are called stray parameters. They can be directly measured by equipment such as an impedance analyzer. According to the condition in electric vehicles, the stray parameters are measured and given as follows: $L_+ = L_- = 120\,\text{nH}$, $R_{g+} = R_{g-} = 0.01\,\text{m}\Omega$, $C_{g+} = C_{g-} = 12\,\text{nF}$.

Since the stray parameters are unrelated to the power battery itself, they do not change with SOC. L_+ and L_- are related to the material, length and shape of the connecting cables. The coupling capacitances are decided by the relative positions among the power battery and the conductors around. Also, all of them change with frequency and have a great effect on the high frequency impedance feature. Based on the tests, measurements and calculations, the parameters of the model in Fig. 5 have been given. They are functions of SOC and frequency. So the model can present the energy dynamic processes and the frequency features at the same time.

4. LEAD ACID BATTERY AND LOW VOLTAGE DEVICES

Lead acid battery and low voltage devices are all loads of the power supply system in electric vehicles. They act as the EMI propagation paths, and their impedance features, especially high frequency impedances, will affect the system EMI characteristics significantly. Also, as sensitive devices, impedances of low voltage devices will influence their immunity.

Firstly, the lead acid battery is discussed. Its impedance can be measured to establish equivalent model and analyze its characteristics [23]. High frequency model of lead acid battery is shown in Fig. 7, where L_b is internal inductance; R_i is internal resistance; R_b and C_b are used to express polarization effects.

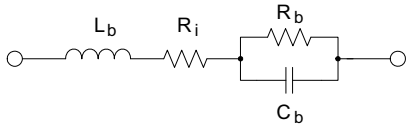

Figure 7. High frequency model of the lead acid battery.

Figure 7 implies the model of the lead acid battery is similar to the power battery. That is because the modeling technology of the power battery is developed based on the research of the lead acid battery. Also, their model parameter identification method is basically the same. Their parameters are all functions of frequency and battery SOC. So the details are not shown here.

Then, BMS is analyzed as the representative of low voltage devices. BMS is used for SOC monitor, voltage balance, over voltage and over current alarms in electric vehicles. A photo of one kind of BMS is shown in Fig. 8(a) and its measured impedance shown in Fig. 8(b). The impedance of BMS is measured by one kind of Agilent

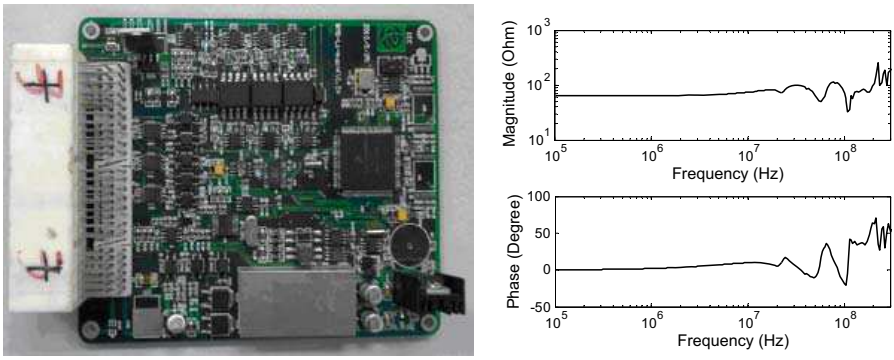

(a) (b)

Figure 8. (a) Photo of the BMS; (b) Measured impedance of the BMS.

impedance analyzer, between the positive terminal and the negative terminal of the BMS without power.

Finally, based on the lead acid battery model and the BMS measured impedance, the impedance features of the loads can be described. They can be combined with models of the converter and the power battery to get the system EMI and analyze the EMI characteristics.

5. SIMULATION AND EXPERIMENT ANALYSIS

Based on the models and analyses above, the power supply system in electric vehicles is modeled to investigate its conducted EMI characteristics. The simulation, experiment verification and analysis contain three parts: the first is the circular current EMI of the paralleled interleaving DC/DC converter; the second is the energy dynamic processes of the system; the last is the system DM and CM interferences. The simulations are conducted through MATLAB, and the experiments are based on an actual electric vehicle. The layout of this electric vehicle is as follows: the power battery is placed in the middle of the vehicle, under the seats, above the vehicle frame; the DC/DC converter is placed in the front of the vehicle, integrated with the inverter in one box, in order to reduce radiation EMI; the lead acid battery is laid near the DC/DC converter in the front of the vehicle; the BMS is placed beside the power battery. The measurement system includes Tektronix oscilloscopes, voltage and current probes to get the waveforms. The spectrums are got through fast Fourier transform (FFT) and calculated by MATLAB.

Firstly, one kind of paralleled interleaving flyback DC/DC converter is selected, which is in the actual electric vehicle used for our experiments. Its output voltage is 13.2–14.5 V to charge the lead acid battery. The controlled power electronics device is MOSFET with the switching frequency 10 kHz. The DM and CM circular currents are shown in Fig. 9.

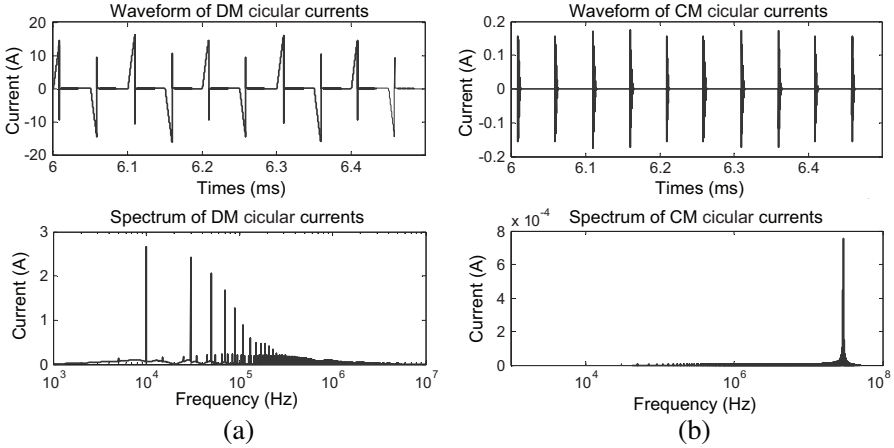

Figure 9. (a) Waveform and spectrum of the DM circular currents; (b) Waveform and spectrum of the CM circular currents

Figure 9(a) shows that the DM circular currents have large peaks which will cause large power losses. At the same time, because the interference flows through a closed annular propagation path, it will lead to radiation emissions which will influence low voltage equipments near the converter. The spectrum of the DM circular currents suggests that the main interference frequencies are the switching frequency of the MOSFETs and its multiples. This proves that the interferences of DC/DC converter are caused by switching processes of the MOSFETs essentially. Fig. 9(b) suggests that the CM circular currents are much smaller than the DM ones. That is because the CM circular currents propagate mainly through the coupling capacitances between the primary and secondary sides of the transformers as inferred in Section 2.3, and the coupling capacitances are always very small. The waveform is represented by a series of resonances, and the main harmonics exist in the resonance frequency of about 40 MHz, which are caused by the coupling capacitances of the transformers and other stray parameters.

Then, the dynamic features of the power battery and system models are studied. The dynamic response of the model in Fig. 5

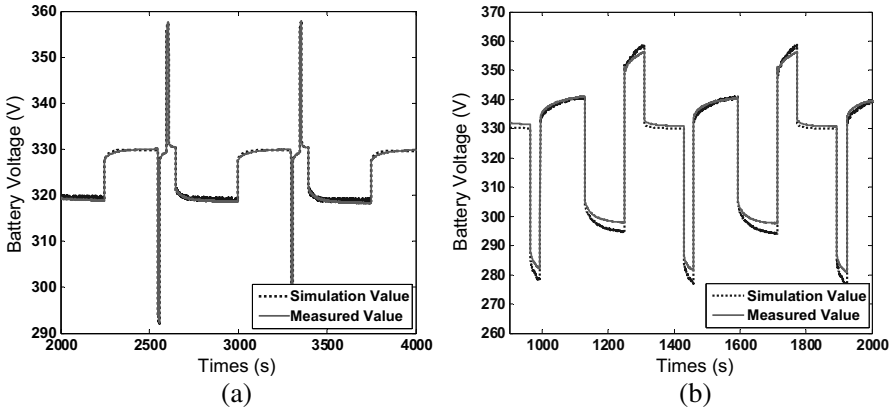

Figure 10. Dynamic response simulation and experiment results, (a) HPPC test, (b) driving circle test.

can be obtained through zero state response and zero input response of the circuit [24]. Also, according to the HPPC test and the dynamic driving circle of electric vehicles, the energy dynamic process of the power battery and the power supply system can be simulated and tested. The results are shown in Fig. 10.

The power battery and system have good dynamic response under HPPC test as shown in Fig. 10(a), while the deviation increases under the driving circle test as shown in Fig. 10(b). That is because of other factors which are not considered, such as temperature, charging rate, etc. However, these factors do not have too much impact, and the simulation values are basically the same as the measured ones. So the models have good dynamic responses when energy storage state changes.

Finally, the system DM and CM EMI are analyzed. Two typical signals are selected to express the system EMI. One is the EMI in the connecting cables between the power battery and the DC/DC converter; the other is the EMI in the connecting cables between DC/DC converter and the loads. These connecting cables all include one positive cable and one negative cable. Defining the currents in the positive cable as i_+ and the currents in the negative cable as i_-, the DM and CM currents can be given by Eq. (7).

$$i_d = (i_+ - i_-)/2, \quad i_c = (i_+ + i_-)/2 \tag{7}$$

So DM and CM EMI in the connecting cables between the power battery and the DC/DC converter are shown in Fig. 11. Also, the ones in the connecting cables between DC/DC converter and the loads are shown in Fig. 12.

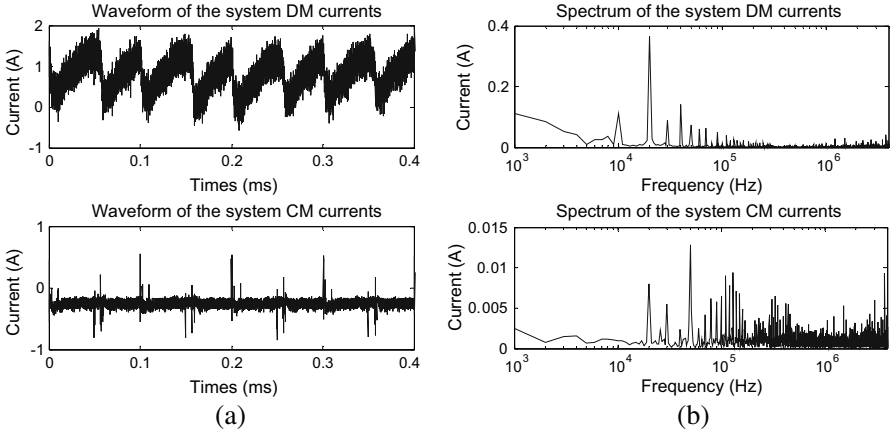

Figure 11. DM and CM EMI in the connecting cables between the power battery and the DC/DC converter, (a) waveforms, (b) spectrums.

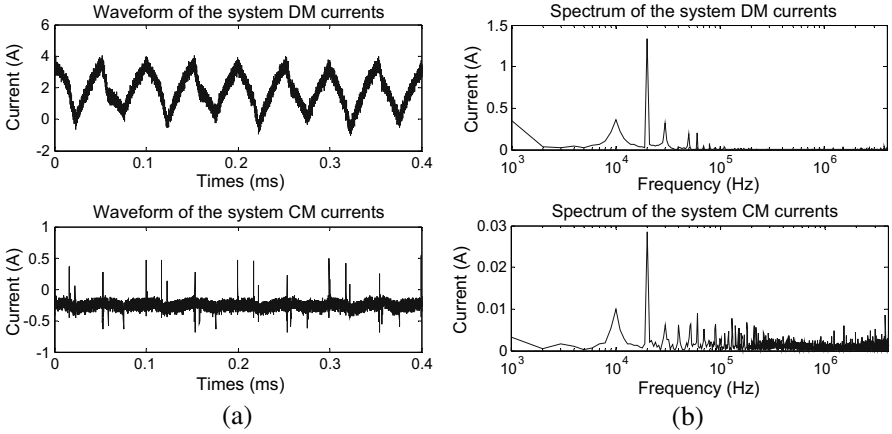

Figure 12. DM and CM EMI in the connecting cables between DC/DC converter and the loads, (a) waveforms, (b) spectrums.

The DM EMI in Fig. 12 has larger current amplitude than the one in Fig. 11. That is because the DC/DC converter changes the input power battery voltage to output voltage 12 V, and the output currents are much larger than the input ones. So the same EMI sources will bring more ripples in the output of the DC/DC converter. Then, the spectrum features of the DM EMI are considered. The harmonics are mainly at the even times of the MOSFET switching frequency. This is caused by the interleaving control as we inferred in Section 2.2, which makes the interference source waveforms of the two paralleled

parts have a phase difference of $\pi/2$. So the EMI sources have more influence on the DM EMI. Besides, the DM EMI spectrum in Fig. 12(b) attenuates faster than the one in Fig. 11(b).

Figures 11 and 12 also suggest that the waveforms of the CM EMI are represented by a series of transient pulses. Their harmonics are at the MOSFET switching frequency and its multiples. However, unlike DM EMI, the amplitude of the harmonics is not attenuated with frequency. It will become large in a certain frequency range. That is caused by the effects of the impedances in the CM propagation paths. So the EMI sources and propagation paths are both important to the CM EMI.

6. CONCLUSION

The model of the power supply system in electric vehicles and its conducted electromagnetic interference characteristics are presented in this paper. The paralleled interleaving DC/DC converter model is established considering both the power electronics devices and the converter topology. Based on the model, the circular current EMI is discussed. Also, a new power battery model is put forward to express the energy dynamic processes and high frequency features at the same time. Furthermore, the impedances of lead acid battery and BMS are shown to estimate effects of the EMI on the loads. Finally, the system model is shown. The dynamic responses, DM and CM EMI are studied through simulations and experiments. The models and analyses shown in this paper can be used for predictions of the time domain and frequency domain EMI characteristics of the power supply system in electric vehicles. They also can help interference suppression and EMC designs in electric vehicles and other power supply systems.

ACKNOWLEDGMENT

Authors gratefully acknowledge the support by Chinese National High-Tech R&D (863 Program) Project (2011AA11A262), National Natural Science Foundation of China (51007088) and International Cooperation Projects funded by MOST of China (2010DFA72760 and 2011DFA70570).

REFERENCES

1. Mahmoudi, A., N. Rahim, and H. Ping, "Axial-flux permanent-magnet motor design for electric vehicle direct drive using sizing equation and finite element analysis," *Progress In Electromagnetics Research*, Vol. 122, 467–469, 2012.

2. Lei, J.-Z., C.-H. Liang, W. Ding, et al., "EMC analysis of antennas mounted on electricity large platforms with parallel FDTD methods," *Progress In Electromagnetics Research*, Vol. 84, 205–220, 2008.
3. Ala, G., M. C. D. Piazza, G. Tinè, et al., "Evaluation of radiated EMI in 42-V vehicle electrical systems by FDTD simulation," *IEEE Trans. on Vehicular Technology*, Vol. 56, No. 4, 1477–1484, July 2007.
4. Lecointe, J.-P., B. Cassoret, and J. Brudny, "Distinction of toothing and saturation effects on magnetic noise of induction motors," *Progress In Electromagnetics Research*, Vol. 112, 125–137, 2011.
5. Jian, L. and K. T. Chau, "Design and analysis of a magnetic-geared electronic-continuously variable transmission system using finite element method," *Progress In Electromagnetics Research*, Vol. 107, 47–61, 2010.
6. Revol, B., J. Roudet, J.-L. Schanen, et al., "EMI study of three-phase inverter-fed motor drives," *IEEE Trans. on Industry Applications*, Vol. 47, No. 1, 223–231, January/February 2011.
7. Akagi, H. and T. Doumoto, "An approach to eliminating high-frequency shaft voltage and ground leakage current from an inverter-driven motor," *IEEE Trans. on Industry Applications*, Vol. 40, No. 4, 1162–1169, July/August 2004.
8. Guttowski, S., S. Weber, E. Hoene, et al., "EMC issues in cars with electric drives," *IEEE International Symposium on Electromagnetic Compatibility*, 777–782, Boston, USA, 2003.
9. Chen, S., T. W. Nehl, J. S. Lai, et al., "Towards EMI prediction of a PM motor drive for automotive applications," *Applied Power Electronics Conference and Exposition*, 14–22, Miami, USA, 2003.
10. Labrousse, D., B. Revol, and F. Costa, "Common-mode modeling of the association of N-switching cells: Application to an electric-vehicle-drive system," *IEEE Trans. on Power Electronics*, Vol. 24, No. 11, 2852–2859, November 2010.
11. Li, W., S. F. Yu, B. Zhang, J. L. He, et al., "High frequency conducted disturbance analysis of driving system in fuel cell vehicle," *The 4th Asia-Pacific Conference on Environmental Electromagnetics*, 724–727, Dalian, China, 2006.
12. Lee, Y. H. and A. Nasiri, "Analysis and modeling of conductive EMI noise of power electronics converters in electric and hybrid electric vehicles," *Applied Power Electronics Conference and Exposition*, 1952–1957, Austin, USA, 2008.

13. Chen, M. and G. A. Rincon-Mora, "Accurate electrical battery model capable of predicting runtime and I-V performance," *IEEE Trans. on Energy Conversion*, Vol. 21, No. 2, 504–511, June 2006.
14. Gao, L., S. Liu, and R. A. Dougal, "Dynamic Lithium-ion battery model for system simulation," *IEEE Trans. on Components and Packaging Technologies*, Vol. 25, No. 3, 495–505, September 2002.
15. Hoene, E., S. Guttowski, R. Saikly, et al., "RF-properties of automotive traction batteries," *IEEE International Symposium on Electromagnetic Compatibility, EMC'03*, 425–428, Istanbul, Turkey, 2003.
16. Meng, J. and W. M. Ma, "Power converter EMI analysis including IGBT nonlinear switching transient model", *IEEE Trans. on Industrial Electronics*, Vol. 53, No. 5, 1577–1583, October 2004.
17. Musumeci, S., A. Raciti, A. Testa, et al., "Switching-behavior improvement of insulated gate-controlled devices, *IEEE Trans. on Power Electronics*, Vol. 12, No. 4, 645–653, July 1997.
18. Guo, Y. J., L. F. Wang, and C. L. Liao, "Systematic analysis of conducted electromagnetic interferences for the electric drive system in electric vehicles," *Progress In Electromagnetics Research*, Vol. 134, 359–378, 2013.
19. Liang, J., L. Jian, G. Xu, et al., "Analysis of electromagnetic behavior in switched reluctance motor for the application of integrated air conditioner on-board charger system," *Progress In Electromagnetics Research*, Vol. 124, 347–364, 2012.
20. Zhang, D., F. Wang, R. Burgos, et al., "DC-link ripple current reduction for paralleled three-phase voltage-source converters with interleaving," *IEEE Trans. on Power Electronics*, Vol. 26, No. 6, 1741–1753, June 2011.
21. Abu-Sharkh, S. and D. Doerffel, "Rapid test and non-linear model characteristsation of solid-state Lithium-ion batteries," *Journal of Power Sources*, Vol. 130, 266–274, May 2004.
22. Hunt, G., "Freedom CAR battery test manual for power-assist hybrid electric vehicles," DOI/ID-11069, INEEL, October 2003.
23. Thelea, M., S. Bullera, D. U. Sauera, et al., "Hybrid modeling of lead-acid batteries in frequency and time domain," *Journal of Power Sources*, Vol. 144, 461–466, June 2005.
24. Dai, H. F., X. Z. Wei, Z. C. Sun, et al., "Online cell SOC estimation of li-ion battery packs using a dual time-scale Kalman filtering for EV applications," *Applied Energy*, Vol. 95, 227–237, July 2012.